Available online at www.eccomasproceedia.org
Eccomas Proceedia COMPDYN (2019) 345-358

ECCOMAS
Proceedia

COMPDYN 2019
7th ECCOMAS Thematic Conference on
Computational Methods in Structural Dynamics and Earthquake Engineering
M. Papadrakakis, M. Fragiadakis (eds.)
Crete, Greece, 24–26 June 2019

UNREINFORCED MASONRY MATERIALS UNDER AXIAL COMPRESSION OR FOUR-POINT FLEXURE. LABORATORY MEASUREMENTS AND NUMERICAL SIMULATIONS

Lampros Kotoulas[1], George C. Manos[2], Lazaros Melidis[3], Kostas Katakalos[4], George Manolis[5]

[1] Lab. Strength of Materials and Structures, Aristotle University
kotoulaslambros@gmail.com

[2,3,4,5] Lab. Strength of Materials and Structures, Aristotle University
gcmanos@civil.auth.gr, lazmelidis@gmail.com, kkatakal@civil.auth.gr, gdm@civil.auth.gr

Abstract

A number of unreinforced masonry walls of prototype dimensions were built at the laboratory of Strength of Materials and Structures of Aristotle University using prototype masonry units together with mortars having such a composition that can be characterized as low strength mortars. The in-plane and out-of-plane behaviour of such structural elements is of considerable interest as existing structures include this type of structural components. During the construction of these piers samples of the mortars used in the construction were taken. After a curing period these samples were subjected to two distinct tests, namely axial compression and four-point bending. Similarly, from the basic material of the masonry units, either clay or natural stone, prismatic specimens were formed which were also subjected to either axial compression or four point flexure. Next, a number of numerical simulations were performed utilizing all the information of the geometry and material characteristics of the mortar or masonry material specimens in order to replicate numerically the axial compression and four point flexure tests which were performed in the laboratory. The numerically simulated behavior resembles the measured brittle load-deformation response and the observed actual damage at the end of the tests. Using back analysis procedures a reasonable correlation can also be achieved between the measured value of the ultimate load and the corresponding value predicted by this type of numerical simulation.

Keywords: Stone and clay masonry, masonry walls, historical construction, weak mortars, in-axial compression, four-point flexure, Numerical Simulations.

ISSN:2623-3347
Peer-review under responsibility of the organizing committee of COMPDYN 2019.
doi: 10.7712/120119.6923.19346

1 INTRODUCTION

A number of unreinforced masonry walls of prototype dimensions were built at the laboratory of Strength of Materials and Structures of Aristotle University using prototype masonry units together with mortars having such a composition that can be characterized as low strength mortars (figure 1).

Figure 1. Masonry walls built with either natural stone or clay bricks and weak mortar

The in-plane and out-of-plane behaviour of such structural elements is of considerable interest as existing structures include this type of structural components. These structural elements behave quite satisfactorily for the vertical gravitational forces. However, they sustain heavy damage when they are subjected to earthquake forces generated from strong ground motions ([1], [2], [3], [4], [5]). This is the main objective of the current investigation.

Figure 2. Old stone masonry church sustained heavy structural damage during the 2014 Kefalonia, Greece, earthquake sequence

Figure 3. Relatively new unreinforced clay masonry infills at the façade of a multi-story reinforced concrete structure. These masonry infills became unstable and collapsed.

This manuscript focuses on the materials used to construct such wall specimens. During the construction of these walls samples of the mortars used in the construction were taken. After a curing period of approximately 2 months these samples were subjected to two distinct tests, namely axial compression and four-point bending. Similarly, from the basic material of the masonry units, either clay or natural stone, prismatic specimens were formed which were also subjected to either axial compression or four point flexure. Details of the experimental sequence are presented in section 2. Summary results and observations of these experimental sequences are presented and discussed in section 3. Next, a number of numerical simulations were performed utilizing all the information of the geometry and material characteristics of the mortar or masonry material specimens in order to replicate numerically the axial compression and four point flexure tests which were performed in the laboratory. The predicted response from these numerical simulations which extend to the non-linear range for both loading sequences is presented in section 4. Comparisons between measured and numerically predicted behaviour is also summarized in this section.

2 FEATURES OF THE EXPERIMENTA SEQUENCE

An extensive experimental sequence was carried out focusing on monitoring basic properties of the materials used to construct the walls of figure 1 in the Laboratory of Strength of Materials and Structures, at Aristotle University. Forming specimens for testing in the laboratory by either casting mortar or forming ceramic or natural stone specimens is relatively an easy task when it is compared with the task of extracting corresponding specimens from existing structural elements in-situ ([5], [6], [7], [8], [9], [10], [11]). A number of non-destructive methods have been developed that together with limited destructive tests can provide the necessary information [9]. This is, however, a special theme that is not discussed further here. Instead, in what follows two relatively simple and very popular testing methods will be employed. The first is referred as ***axial compression*** and it involves placing a cubic or prismatic

specimen with specific dimensions within two horizontal stiff steel plates of a testing machine. The test specimen is initially simply resting on the bottom steel plate having all the rest of its sides free from any constrain. During testing the top steel plate initially makes contact with the top horizontal side of the specimen; then it continues moving downwards in a controlled way, exercising in this way a axial compression that is usually measured as a resultant compressive force. A common assumption made is that this axial force results in a uniform axial compressive stress distribution at a horizontal cross section of the specimen; this cross-section is assumed to be located at a vertical distance far from the top and bottom support steel plates in order to be free of any boundary disturbances. The ultimate value of this compressive axial load results in the compressive strength of the specimen. The second testing process, termed ***flexural test***, is shown in figure 4. A prismatic specimen having the prescribed dimensions is placed on the testing machine as shown in this figure [5]. The bottom steel cylindrical supports of this specimen are resting on a stiff steel horizontal plate of the testing machine rigidly so that it is assumed for them a zero vertical displacement regime. The top horizontal steel plate of the testing machine initially makes contact with the top steel cylindrical part that simple rests on top of the specimen. The test arrangement in figure 4 has this steel cylinder placed at the middle of the clear span of the tested specimen. By moving the top horizontal steel plate of the machine downwards in a controlled way a vertical force is applied at mid-span of the test specimen. Through this test arrangement and assuming that the applied vertical load is equilibrated only by two equal vertical forces at the two supports with a value equal to ½ of the centrally applied load the distribution of the bending moment and shear force in the region of the specimen between the two supports is assumed to be known according to the classic elastic beam theory. Following similar classic elastic beam theory assumptions on the distribution of axial stress at a vertical mid-span cross section the bottom fiber axial stress is associated with the maximum value of the bending moment resulting from the ultimate load measured during testing. In this way, the tensile flexural strength is found. This is the main objective of this testing arrangement which is used for defining this type of tensile strength (flexural) for mortar, natural stone, or burnt clay ceramic material found in man made masonry units. It is known that these materials, as well as other materials like concrete, have compressive strength much larger than the corresponding tensile strength. Therefore, this test is a simple way for determining such a “flexural” tensile strength. For these relative “weak-in-tension” materials the determination of the “direct” tensile strength is relatively more difficult in comparison. An indirect test method for defining the tensile strength that is also reported, which is also relatively simple, is the so called “Brazilian” test. A number of more complex tests have also been employed in order to define the strength of these materials in a 2-D stress filed; however, these test methods are beyond this investigation at present.

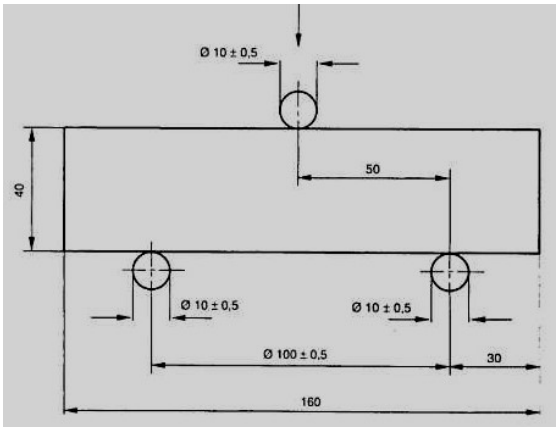

Figure 4. Three-point-bending testing arrangement according to EN 1015-11 [5]

The common name for the previously described test (figure 4) is '***three point bending***" associated with these used during testing three steel cylinders (two supports at the bottom and one in the middle applying the central vertical force). This testing procedure is described in detail in various EN 1015-11 "Methods of test for mortar for masonry Ð Part 11: Determination of flexural and compressive strength of hardened mortar" [5]. Another simple alternative from that shown in figure 4 is replacing the single cylinder placed at mid-span at the top of the specimen by two equally spaced cylinders also placed at the top. In this way the total clear span is divided in three parts with the central mid-third part being free, according to the classic elastic beam theory, of any stress filed from internal shear forces. In this case, the only stress filed which develops in this central mid-third part is that resulting from the corresponding internal bending moment regime. Thus, the flexural tensile strength can again be derived in a similar way. This time, the common name for this alternative test (figure 5) is '***four point bending***" associated with these used during testing four steel cylinders (two supports at the bottom and two at the top applying symmetrically the central vertical force). The common form of failure associated with either the three or the four-point-bending testing is depicted in figure 6. It is important for both the axial compression and the flexural tests to properly place the specimens on the testing machine and to ensure that either the supports of the loading plates and fixtures do not create any parasitic stress field that could influence the observed behaviour. As already described, the main information that is derived from these tests is the compressive strength and the flexural tensile strength based on the recorded applied maximum load and the relevant cross-section of the specimen.

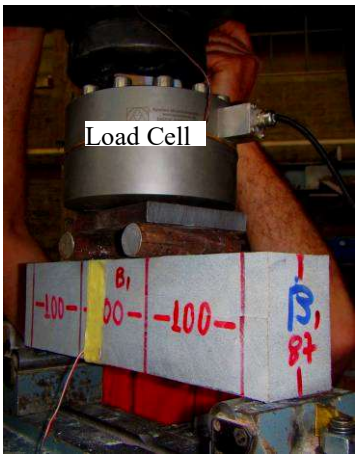

Figure 5. Four point bending testing arrangement

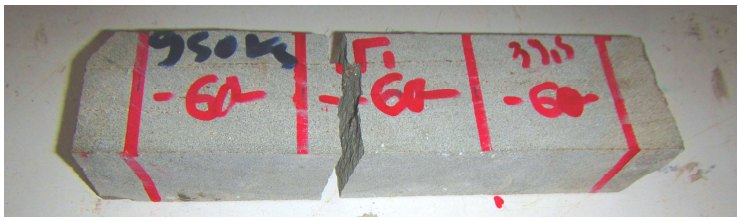

Figure 6. Failure mode of a natural stone specimen resulting from "Four point bending testing arrangement".

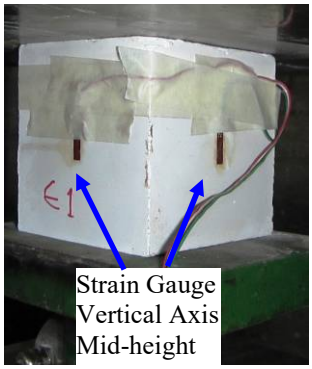

Figure 7a. Mortar axial compression

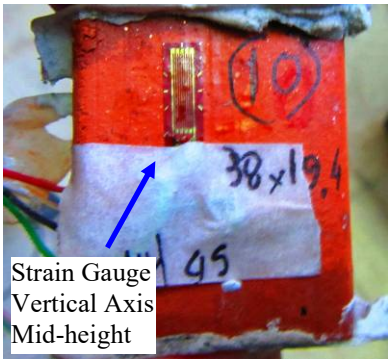

Figure 7b. Ceramic material axial compression

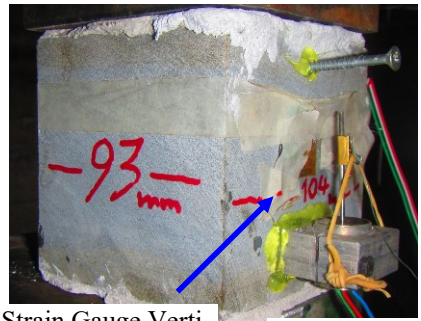

Figure 7c. Natural stone axial compression

Additional instrumentation can be placed to monitor the deformability parameters of the tested specimens. One relative simple way for this objective is to place displacement or strain sensors at the visible parts of a specimen. This is shown in figures 7a, 7b and 7c for the axial compression specimens during tests with mortar, ceramic material or natural stone, respectively. In figures 7a and 7b strain gauges are placed at mid-height of one side corresponding to one vertical plane of symmetry of each specimen. Three additional strain gauges can be placed at the corresponding locations for the remaining three sides to augment the accuracy of this deformability recording. All these strain gauges aim to capture the variation of the axial strain with the gradual application of the axial compressive load applied to the specimen during this test. Figure 7c depicts the testing arrangement of a natural stone specimen whereby a sensitive small displacement transducer has been placed on one side to monitor the relative axial deformation between two points at this side located at the vertical plane of symmetry. In addition a strain gauge with one vertical and on horizontal component has also being placed on the same side. Again, three additional strain gauges and three additional displacement transducers can be placed at the corresponding locations for the remaining three sides to augment the accuracy of this deformability recording.

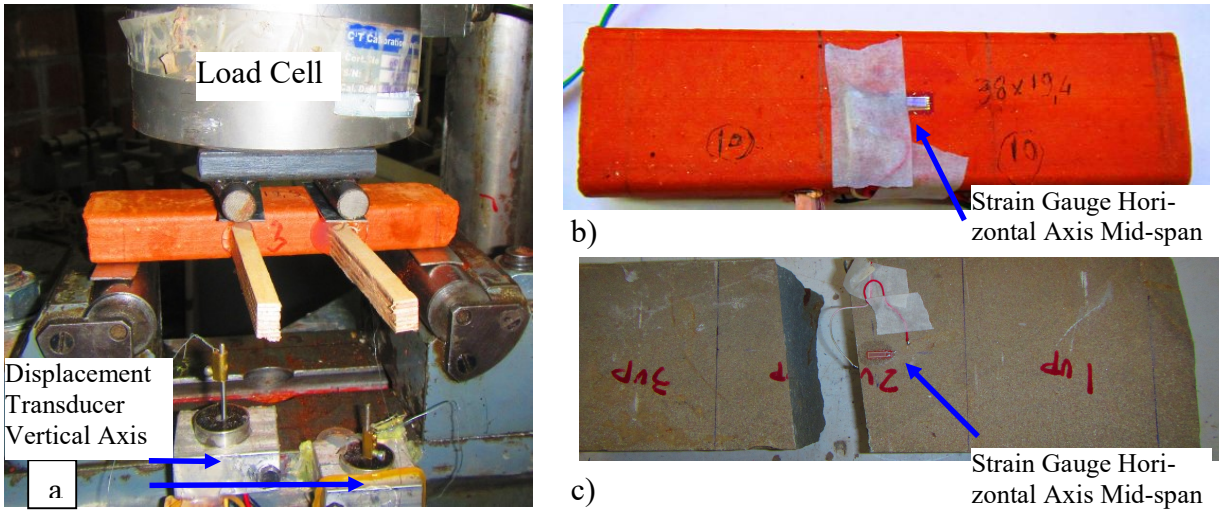

Figure 8. Four-point-bending test. Measuring devices. a) Ceramic material displacement transducers b) Ceramic material strain gauges c) natural stone strain gauges.

Figures 8a, 8b and 8c depict instrumentation scheme for measuring the applied load together with the deformability of specimens subjected to four-point-bending. In figure 8a two sensitive displacement transducers have been placed to record the vertical displacement of the tested ceramic specimen at two points located at the central mid-third of the total span. Figures 8b and 8c depict the strain gauges at mid-span of the top fiber, oriented in the horizontal direction located at the vertical plane of symmetry, of each specimen. An additional strain gauge is also located at the mirror opposite location at the bottom fiber of each specimen. These strain gauges are aimed to capture the variation of the corresponding axial strain in the longitudinal direction, at the top and bottom fibers due to the flexure, with the gradual increase of the central vertical load applied to the specimen during this test.

For both the axial compression and the flexure tests using more than one displacement and strain sensor can compensate for the development during tests parasitic non-symmetric deformation patterns. The general limitation of all these measuring schemes lies to the fact that after a certain load level the behaviour seizes to be elastic. This is particularly magnified after when the ultimate load is reached. It becomes very dominant when at declining branch of the load-deformation curve of the response when the cracks and broken pieces of the tested mate-

rial become visible. In this case, the assumptions of symmetric small amplitude axial strain and deformation distributions based on the elastic theory are not anymore valid. Thus, such an instrumentation scheme cannot capture all the fracture phenomena that occur at this stage which may have a non-symmetric and local character.

3 RESULTS AND OBSERVATION FROM THE MEASURED BEHAVIOUR

3.1. Axial compression test

Figure 9 depicts the stress-strain response derived form the load, deformation and strain measurements of the stone prism shown in figure 7c obtained when this specimen was subjected to axial compression. Three sets of strain measurements are included in this figure.

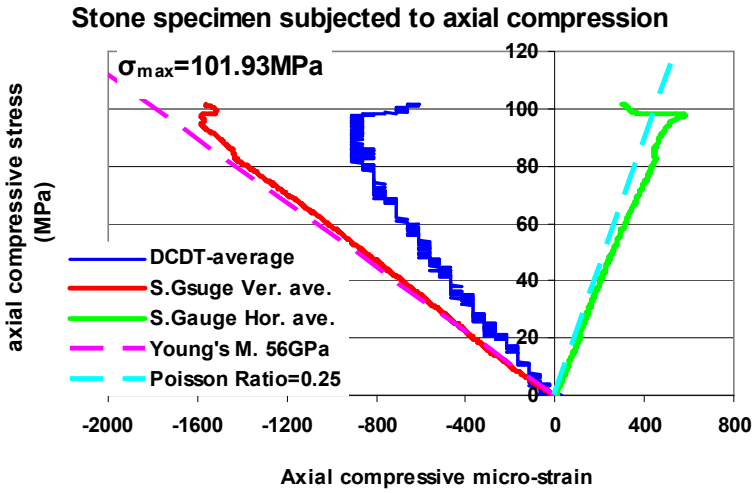

Figure 9. Stress-strain response from the measurements obtained during the axial compression tests of a natural stone prismatic specimen.

Figure 10. The failed stone specimen. Notice the dislocation of the displacement transducers and the debonding of the strain gauges at this final stage of testing.

The first set of plotted strains is derived from the average of the axial strain readings measured through the strain gauges oriented in the vertical directions at the mid-height of the sides of the stone prism, as described in section 2. The axial compressive stress values are plotted

with a positive sign whereas the positive is potted the strain from axial extension. The second set of plotted strains was derived from the average of the axial strain readings measured through the strain gauges oriented in the horizontal directions at the mid-height of the sides of the stone prism, as described in section 2. The third set of plotted strains was derived from the average of the vertical displacement readings measured by the displacement transducers oriented in the vertical direction at the sides of the stone prism, as described in section 2. Figure 10 depicts the failed specimen at the end of the test sequence. The axial compressive strength is equal to 101.93MPa. From the measured axial stress versus axial strain response in the vertical direction, based on the strain gauge measurements, the value of the Young's modulus is derived. The strain response based on the measured displacement transducers reading is approximately 50% smaller than the strain response based on the strain gauge readings. Finally, by combining the strain readings along the vertical and the horizontal direction, as they were recorded through the strain gauge output, the value of the Poisson's ratio is derived.

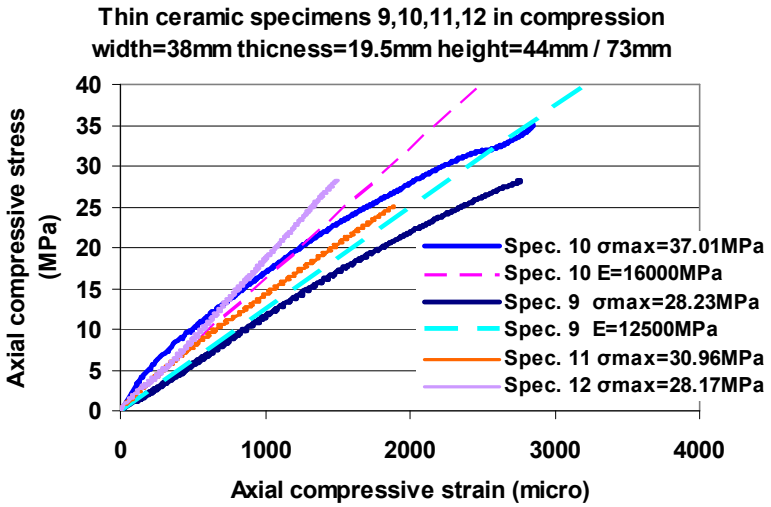

Figure 11. Stress-strain response from the measurements obtained during the axial compression tests of prismatic specimens made with ceramic material.

Figure 11 depicts the stress-strain response derived form the load and strain measurements of the ceramic prism shown in figure 7b obtained when a number of specimens was subjected to axial compression. Only the strain measurements obtained by the attached vertically oriented strain gauges are included in this figure. The average compressive strength of these ceramic specimens is equal to 33.532MPa. The obtained Young's modulus value ranges between 12.5GPa and 16.0GPa. As already discussed, when the ultimate load (stress) is reached and a sudden reduction of the load capacity is observed together with a large increase in the deformation of the specimens accompanied by visible cracks. This behaviour is characteristic of brittle materials like the ones examined here. It characterizes both the axial compression behaviour as well as the flexural behaviour which is presented in section 3.2. The employed sensors cannot capture this type of deformation and strains at this stage of the axial compression test with an acceptable degree of approximation. This is the reason that the plotted response in figures 9 and 11 does not extend beyond the ultimate load range.

3.2. Four-point bending test

Results form the four-point-bending test with the ceramic specimen depicted in figures 8a and 8b will be presented and discussed here. Figure 12a the variation of the flexural tensile stress with that of the vertical deflection at mid-span. It can be seen that the gradual increase of the

applied load, and the corresponding flexural tensile stress results in relatively small deflection values up to the point where the ultimate stress (load) is reached. Then, the sudden reduction of the bearing capacity is accompanied by the considerable increase of the measured deflection, which as discussed is characteristic of the brittle behaviour. Similarly, figure 12b displays the variation of the flexural tensile stress with the variation of the measured by the strain gauges top and bottom fiber axial strains. It can be seen that the bottom fiber strain exhibits a non-linear variation with the flexural axial stress which becomes more pronounced when the ultimate load is reached.

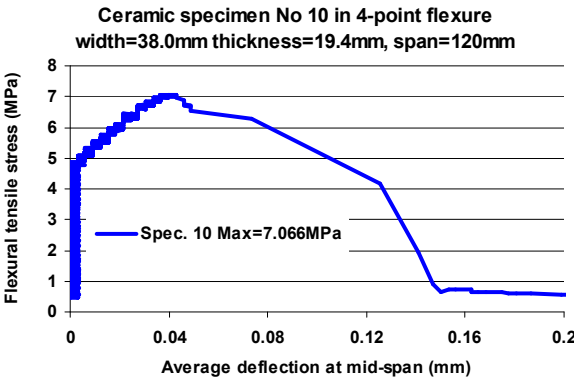

Figure 12a. Flexural tensile stress versus vertical deflection at mid-span

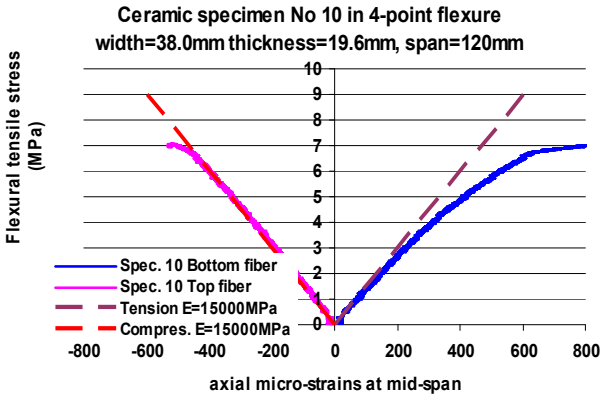

Figure 12b. Flexural tensile stress versus axial strain of top and bottom fiber at mid-span

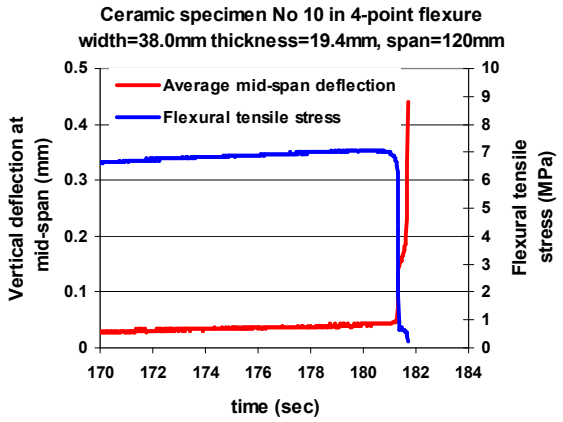

Figure 13a. Variation of the Flexural tensile stress and the vertical deflection at mid-span after the ultimate load is reached

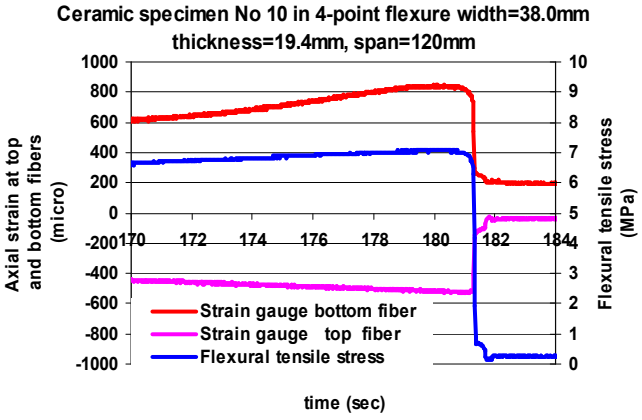

Figure 13a. Variation of the Flexural tensile stress and the top and bottom fiber axial strains at mid-span after the ultimate load is reached

Figures 13a and 13b are also characteristic of the observed brittle behaviour as this was captured by the measurements during testing. In both figures the variation of the applied load in time is shown through the variation of the flexural tensile stress. From the total loading duration only the last 14 seconds when the ultimate load was reached are depicted. It can be seen in figure 13a that the sudden reduction of the flexural tensile stress is accompanied by the sudden increase of the vertical deflection at mid-span (flexural mode of failure, figure 8c), characteristic of the brittle behaviour. In figure 13b it can be seen that reaching the ultimate flexural tensile stress and before the failure of the specimen (sudden reduction of the flexural

tensile stress) the recorded by the bottom fiber strain gauge axial strain appears to demonstrated a noticeable increase. Then, with the sudden reduction of the load (flexural failure, figure 8c) both bottom and top fiber axial strain measurements are also exhibit a similar sudden decrease.

4 NUMERICAL SIMULATIONS OF THE OBSERVED BEHAVIOUR

4.1. Numerical simulation of the axial compression test

A three dimensional (3-D) finite element representation of the axial compression test was formed through the commercial software ([12], [13]) as shown in figure 14a. The loading and boundary conditions try to simulate the axial compression test described in sections 2 and 3.1. The numerical simulation of the top and bottom steel plates were connected with the numerical simulation of the axial compression specimen with numerical "contact" surfaces. Various non-linear constitutive laws included in this commercial software were tried; results from the constitutive law "concrete damage plasticity" are presented here. The presented results depicted in figures 14b and 14c are plots of the distribution of plastic strains within the volume of the numerical simuation. Figures 14b and 14c show the distribution of the plastic strain within the volume of the specimen before and after the ultimate load is reached, respectively.

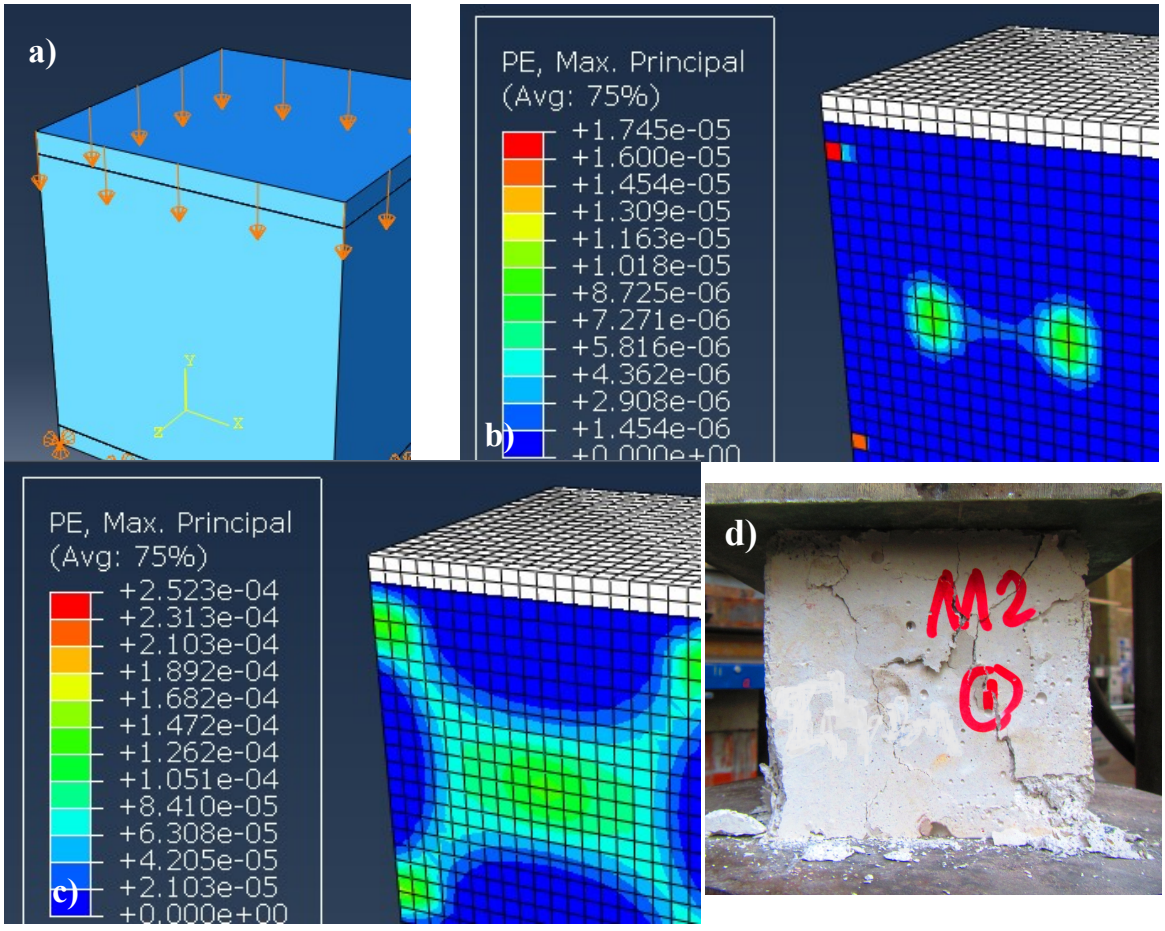

Figure 14. Numerical simulation of the axial compression tests. Comparison of numerically predicted (c) and observed (d) damage patterns.

Figure 14d is the failure mode of a mortar cube with visible the main cracking patterns, which resemble the distribution of the plastic strains after the ultimate load is reached, shown in figure14c, as he corresponding numerical predictions of the observed damage.

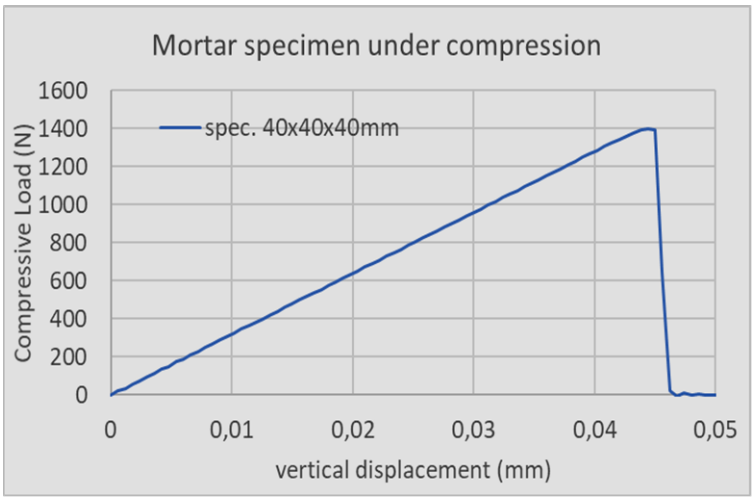

Figure 15. Numerical simulation of the variation of the axial compressive load versus the vertical deformation of the cubic specimen of figure 14a. tests.

Figure 15 depicts the variation of the axial compressive load versus the corresponding vertical deformation of the numerical simulation of the axial compressive test with the cubic specimen of figure 14a. As can be seen in this figure, the brittle nature of the compressive behaviour is clearly represented by this load versus displacement curve. Through a sensitivity analysis it was found that the described numerical simulation depends on the choice of the time step for the non-linear integration as well as on the parameters that define the employed non-linear constitutive law. Using back analysis procedures a reasonable correlation can be achieved between the measured value of the ultimate compressive load and the corresponding value predicted by this type of numerical simulation.

4.2. Numerical simulation of the four-point-bending test

As was done for the axial compressive test on section 4.1, a three dimensional (3-D) finite element representation of the four-point-bending test was formed through commercial software ([12], [13]) as shown in figure 16a. The loading and boundary conditions try to simulate the actual four-point-bending test described in sections 2 and 3.2. The numerical simulation of the bottom cylindrical supports as well as the top cylinders for applying the vertcal load were reprented with rigid prism as shown in figure 16.

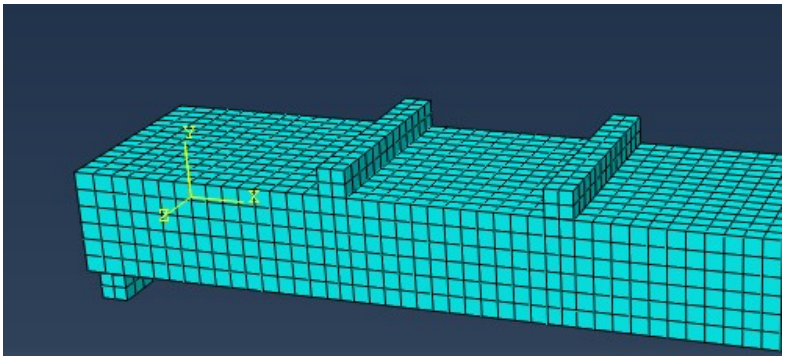

Figure 16. Numerical simulation of the four-point-bending test.

These rigid prisms were connected with the numerical simulation of the specimen with numerical "contact" surfaces. Again, various non-linear constitutive laws included in this commercial software were tried; results from the constitutive law "concrete damage plasticity" are presented here. Figure 17a depicts the distribution of plastic strains within the volume of the numerical simuation of the four-point-bending specimen after the ultimate load is reached. Figure 17b is the failure mode of the ceramic specimen subjected to four-point-bending with the main wide crack going through the central mid-third part of the specimen, as presented and discussed in sections 2 and 3.2. As can be seen from these figures, the actual damage shown in figure 17b resembles the distribution of the plastic strains after the ultimate load is reached, shown in figure17a, as he corresponding numerical predictions of the observed damage.

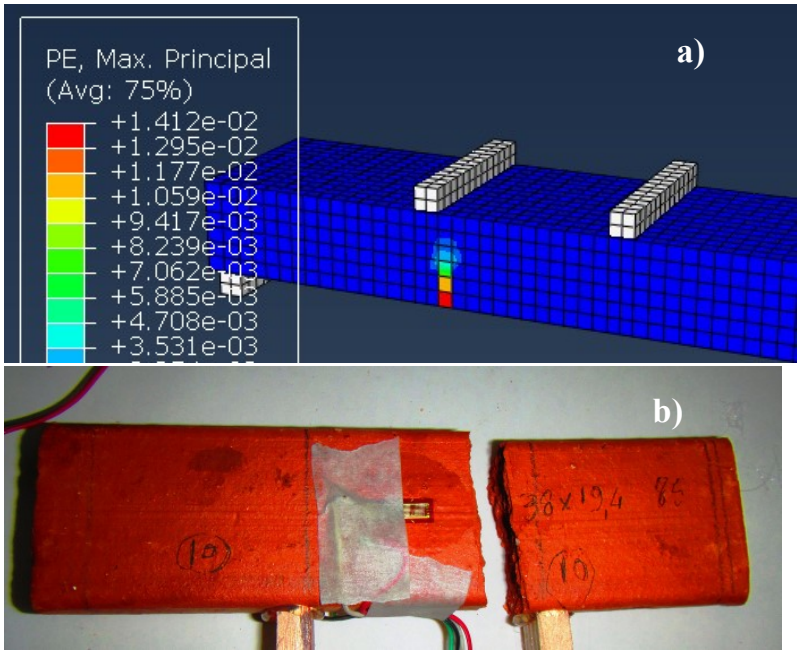

Figure 17. Comparison of numerically predicted (a) and observed (b) damage patterns.

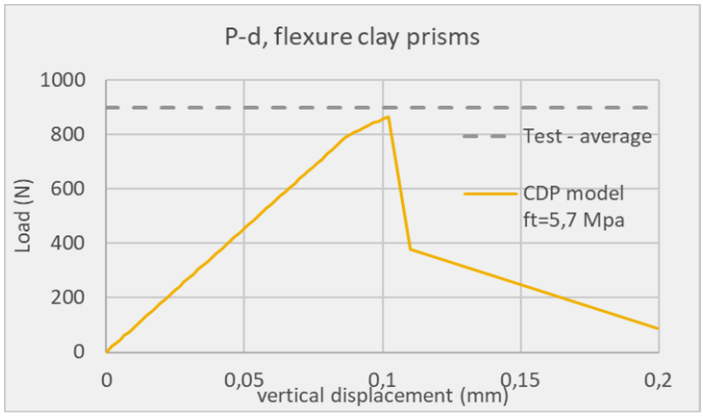

Figure 18. Numerical simulation of the variation of the total vertical applied to the four-point-bending specimen load versus the vertical deflection at mid-span.

Figure 18 depicts the variation of the applied total vertical load versus the corresponding vertical deformation at mid-span as predicted by the numerical simulation of the four-point

bending test (figure 16) with the prismatic specimen of figure 8a. As can be seen in this figure, the brittle nature of the compressive behaviour is represented by this load versus displacement curve. Again, through a sensitivity analysis it was found that the described numerical simulation depends on the choice of the time step for the non-linear integration as well as on the parameters that define the employed non-linear constitutive law. Using back analysis procedures a reasonable correlation can be achieved between the measured value of the ultimate compressive load (figures 18 and 19) and the corresponding value predicted by this type of numerical simulation.

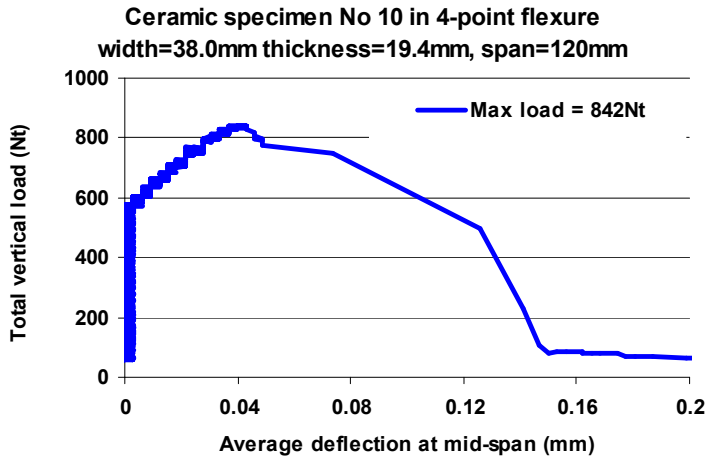

Figure 19. Measured variation of the total vertical applied to the four-point-bending specimen load versus the vertical deflection at mid-span.

5 CONCLUSIONS

- The mechanical characteristics of basic materials, used in the construction of masonry made either by natural stone or ceramic units, are investigated. This is done employing simple tests commonly used to defining the axial compressive strength and the flexural tensile strength in the laboratory.
- A number of mortar specimens were studied together with specimens formed by natural stone or ceramic material. All these specimens were subjected to either axial compression or four-point-bending tests in the laboratory recording the brittle nature of their behaviour together with the corresponding axial compression or flexural tensile strength.
- A 3-D finite element simulation of either the axial compression or the four-point-bending test was formed utilizing the capabilities of commercial software. In both numerical simulations all the geometrical, loading and support details of these tests were numerically simulated. The numerical simulation presented here adopted in both cases the “concrete damage plasticity” constitutive law in an effort to numerically simulate the observed behaviour.
- As can be seen, by comparing the numerically simulated behavior with the one observed, the measured brittle load-deformation response was successfully captured by these numerical simulations. Moreover, the observed actual damage at the end of the tests resembles the distribution of the plastic strains after the ultimate load is reached, as predicted by these numerical simulations.

- Using back analysis procedures a reasonable correlation can also be achieved between the measured value of the ultimate load and the corresponding value predicted by this type of numerical simulation.

ACKNOWLEDGEMENTS

Part of the aforementioned research has been co-funded by Greece and European Union through the Operational Program "Erevno-Dimiourgo-Kainotomo" T1EΔK-03314 which are gratefully acknowledged

REFERENCES

1. Manos G.C., (2011) "Consequences on the urban environment in Greece related to the recent intense earthquake activity", *Int. Journal of Civil Engineering and Architecture*, Dec. 2011, Volume 5, No. 12 (Serial No. 49), pp. 1065–1090.
2. Manos G.C., Nick Simos N. and Kozikopoulos E. (2016) "The Structural Performance of Stone-Masonry Bridges", Chapter 4, "Structural Bridge Engineering", ISBN 978-953-51-2689-8, Print ISBN 978-953-51-2688-1, http://dx.doi.org/10.5772/64752.
3. Manos G.C., "The Seismic Behaviour of Stone Masonry Greek Orthodox Churches" Journal of Architecture and Engineering, Vol. 1, Issue 1, March 2016, pp. 44-53.
4. Manos, G.C and Kotoulas, L. (2017), "Unreinforced stone masonry under in-plane state of stress from gravitational and seismic actions. Measured and predicted behaviour", *COMPDYN 2017*, Rhodes Island, Greece, June 2017
5. EUROPEAN STANDARD EN 1015-11, (2006), "Methods of test for mortar for masonry Ð Part 11: Determination of flexural and compressive strength of hardened mortar, December 2006.
6. EUROPEAN STANDARD EN 772-1, (2011), "Methods of test for masonry units - Part 1: Determination of compressive strength, May 2011
7. Eurocode 6, (2005), "Design of masonry structures - Part 1-1: General rules for reinforced and unreinforced masonry structures".
8. Binda L., RILEM Committees, RILEM TC127-MS: Tests for masonry materials and structures, Materials and Structures, Vol. 29, pp. 459-475, 1996.
9. Binda L., de Vekey R. RILEM TC 177-MDT Workshop: On Site Control and Non Destructive Evaluation of Masonry Structures, Materials and Structures, Vol. 35, pp.443-444, 2002.
10. Tasios, T. P. , (1987), "The Mechanics of Masonry", Athens, (in Greek)
11. Tasios, T. P. (2013), "Parameters affecting the compressive strength and critical strain of masonry", *SEMINARIO SUL TEMA: "EVOLUZIONE NELLA SPERIMENTAZIONE PER LE COSTRUZIONI"*, Centro Internazionale di Aggiornamento Sperimentale – Scientifico, pp. 191-212, Crete-Greece.
12. SAP2000, Integrated Software for Structural Analysis and Design, Computers and Structures Inc.
13. Abaqus Unified FEA - SIMULIA™ by Dassault Systèmes